THE JOURNAL OF PHYSICAL CHEMISTRY C

C: Energy Conversion and Storage; Energy and Charge Transport

Ether Group Mediated Aqueous Proton Selective Transfer Across Graphene-Embedded 18-Crown-6 Ether Pores

Le Shi, Ao Xu, and Yonghong Cheng

J. Phys. Chem. C, **Just Accepted Manuscript** • DOI: 10.1021/acs.jpcc.9b09715 • Publication Date (Web): 18 Oct 2019

Ether Group Mediated Aqueous Proton Selective Transfer across Graphene-Embedded 18-Crown-6 Ether Pores

Le Shi, †, Ao Xu‡, Yonghong Cheng†*

†State key Laboratory of Electrical Insulation and Power Equipment, Center of Nanomaterials for Renewable Energy, School of Electrical Engineering, Xi'an Jiaotong University, Xi'an 710049, China

‡School of Aeronautics, Northwestern Polytechnical University, Xi'an 710072, China

* Corresponding Author. Email: le.shi@mail.xjtu.edu.cn (Le Shi)

ABSTRACT

Nanoporous 2D materials provide a new avenue for the design of zero-crossover proton selective membrane, which is critical for the development of direct methanol fuel cells and many other renewable energy systems. In this work, we investigate the aqueous proton selective conduction behavior across graphene-embedded 18-crown-6 ether pores using extensive ReaxFF molecular dynamics simulations. It is found that though there exist a vacuum gap between the aqueous phase and graphene membrane, the proton conduction behavior can be mediated by the crown ether functional groups and result in a low proton penetration energy barrier of 5.53±0.29 kcal mol^{-1}, corresponding to a high proton conductivity of about 3.23×10^{5} S cm^{-2}. Meanwhile, the vacuum gap together with the small pore size can effectively block the transportation of other molecules such as methanol, resulting in a high proton-methanol selectivity of about 9.3×10^{25}. Our results indicate that functional groups can significantly influence the proton conduction behavior across nanoporous 2D materials, and graphene membrane with embedded 18-crown-6 ether pores is a promising candidate for zero-crossover proton exchange membrane.

TOC GRAPHICS

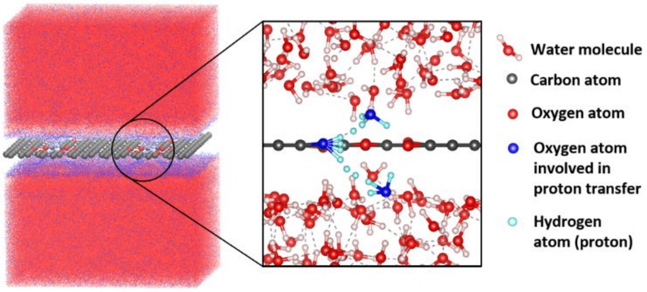

KEYWORDS

Graphene, Crown ether, Proton conduction, Proton-exchange membrane, Direct methanol fuel cell

1. INTRODUCTION

Since the first discovery of graphene in 2004,[1] two-dimensional (2D) materials has becoming a new family of building blocks for membranes due to their unique atomic structure.[2-4] By creating pores on 2D materials, selective mass transport at nanoscale can be achieved, which has found broad applications in gas separation, water desalination, sensing, and so on.[5-7] In 2014, Geim *et al.* proposed that the uniform pores formed by the electron clouds of graphene and *h*-BN can allow the penetration of proton while block the transportation of any other species.[8] This discovery opened up a new avenue for the design of zero-crossover proton exchange membrane, and is particularly important for the development of direct methanol fuel cells (DMFCs) where methanol crossover can poison the noble metal catalyst in the cathode side thus severely deteriorating the cell performance.[9] Follow-up experimental work shown that when sandwiching a single layer of graphene in Nafion membrane, the methanol crossover phenomenon can be greatly reduced.[10-12]

However, how protons conduct across 2D materials such as graphene and *h*-BN is controversial. Many theoretical[13, 14] and experimental work[15] show that the energy barriers for aqueous proton conduction across pristine graphene or *h*-BN are too high to be realized at room temperature, and the previously observed proton conductivity may come from the contribution of atomic defects or bias potential. In our previous work, we investigated the relationship between proton conduction capability and the pore size of nanoporous 2D graphyne.[16] We found that when the side length of the triangular pores in graphyne is smaller than 1.2 nm, a vacuum gap exists between the aqueous phase and graphyne, making proton conduction hard to be realized at room temperature. When the side length is larger than 1.2 nm, protons can transport *via* Grotthuss mechanism along the "water wires" penetrating graphyne with a high conductivity. It should be noted that graphyne is a simplified model of nanoporous 2D materials with inert acetylenic pore edges, while in practical applications, the pore edges of nanoporous 2D materials can be decorated by different kinds of functional groups.[17-19] The relationship between functional groups and proton conduction behavior is yet to be understood. When preparing nanoporous 2D materials, one of the most popular way is to create nanopores on graphene.[2] Guo *et al.*[20] observed that the residual oxygen atoms in oxidized graphene form highly stable crown ether configurations within the 2D graphene layer. The graphene-embedded crown ether pores are predicted to show unique ion adsorption behavior towards K^+ ions, making it a promising choice for ion-based logical elements[21] and strain-controllable ion sieving devices.[7, 22] When serving as proton exchange membrane, the presence of ether functional groups may change the hydrogen bond network in aqueous environment, thus influencing the proton conduction behavior. In this work, we explored the proton selective transfer behavior across graphene embedded 18-crown-6 ether pores (as shown in Figure 1) using extensive reactive force field molecular dynamics (ReaxFF MD) simulations. The recently developed CHON-2017_weak ReaxFF force field[23, 24] was employed to accurately describe the weak interaction of functionalized hydrocarbon/water molecules in condensed phase and capture the Grotthuss hopping proton motion.[25] From the ReaxFF MD simulations, we found that though the pore size is very small and there exist a vacuum gap between the aqueous phase and graphene membrane, the ether functional groups can mediate the proton transfer process and significantly lower the proton conduction energy barrier to 5.53 kcal mol^{-1}, which corresponds to a high area normalized proton conductance of 3.23×10^5 S cm^{-2}. In the meantime, the vacuum zone together with the small pore size can effectively block the transfer of methanol molecules, providing an ultrahigh proton-methanol selectivity of 9.3×10^{25}. This proton selective conduction phenomenon cannot be observed in graphene pores terminated with carbon or hydrogen atoms. Our findings demonstrated the significant influence of functional groups towards aqueous proton transfer behavior, and shed light on future designs of zero-crossover proton exchange membrane based on nanoporous 2D materials.

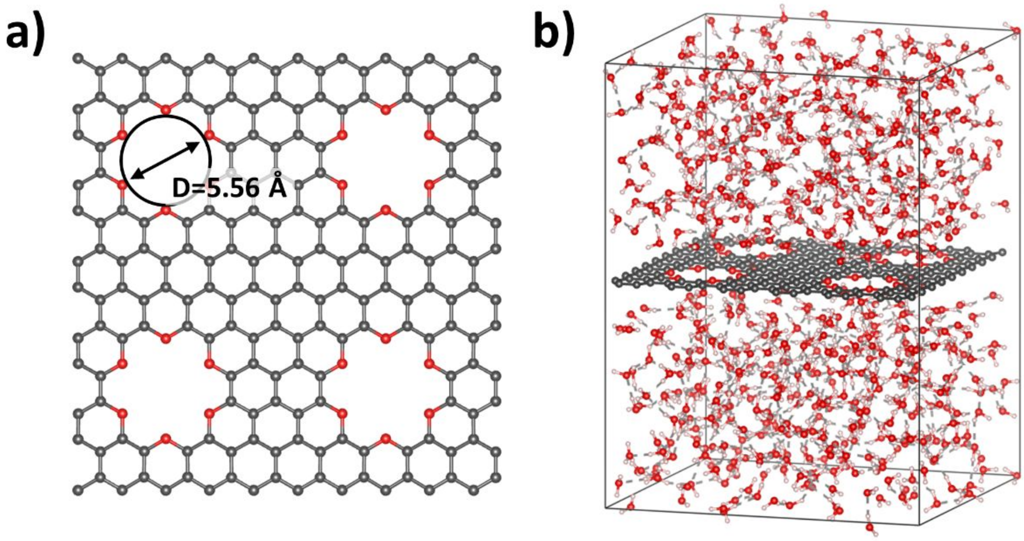

Figure 1. Geometry of graphene embedded 18-crown-6 ether pores in (a) vacuum and (b) aqueous environment.

2. METHODOLOGY

2.1 DFT calculations. All the DFT calculations were performed using Abinit software package.[26-28] Perdew-Burke-Ernzerhof (PBE) generalized gradient approximation (GGA)[29] was adopted as the exchange correlation functional and projector-augmented-wave method was use to describe the electron-ion interaction.[30] The cutoff energy was set to be 20 Ha, and the k-point mesh was set to be <0.05 $Å^{-1}$. All the structures were fully optimized to reach a force tolerance of 0.01 eV $Å^{-1}$.

2.2 ReaxFF MD simulations. The CHON-2017_weak ReaxFF force field parameters[23, 24] was used for all the MD simulations. All MD simulations were performed using LAMMPS[31, 32] software. For all production ReaxFF MD simulations, the time step is 0.25 fs and the Nosé-Hoover chains thermostat was used with a pressure and temperature damping constant of 1000 and 100 fs for the *NPT* and *NVT* MD simulations, respectively. For metadyanmics[33] simulations, PLUMED plugin[34] was used to deal with the proton hopping process. The Guassian hills were deposited every 100 MD steps. The height and width of Guassian hills were 0.05 kcal mol^{-1} and 0.5 Å respectively.

For proton penetration across graphene membrane with embedded crown ether pores, proton hops between water molecules through Grotthuss mechanism. The Collective Variable (CV) is defined as the distance L between the oxygen atom in the hydronium ion $\boldsymbol{r}_O(t)$ and graphene membrane:[16, 35, 36]

$$L = r_O(z) - g(\mathrm{z}) \qquad \text{(Eq. 1)}$$

where $r_O(z)$ can be calculated using:

$$r_O(z) = \frac{\sum_{i \in \{O_w\}} z_i e^{\lambda n_i}}{\sum_{i \in \{O_w\}} e^{\lambda n_i}} \qquad \text{(Eq. 2)}$$

where z_i is the z position of waters' or hydronium's oxygen i, λ is a large number (we set as 100 in our computation), and $\{O_w\}$ refers to all oxygen atoms in the simulation system. The variable n_i is the hydrogen coordination number:

$$n_i = \sum_{j \in \{H_w\}} n(r_{ij}) \qquad \text{(Eq. 3)}$$

where $\mathrm{n}(r_{ij}) = \frac{1-(\frac{r_{ij}}{r_0})^6}{1-(\frac{r_{ij}}{r_0})^{12}}$, r_{ij} is the distance between oxygen atom i and hydrogen atom j, and $\{H_w\}$ refers to all hydrogen atoms in the simulation system. The variable r_0 is set to be 1.25 Å. The variable n_i is very close to 3 when i is the oxygen atom of the hydronium ion and 2 in the case of a water molecule.

For methanol penetration, the CV was chosen as the distance L between the carbon atom in the methanol molecule $\boldsymbol{r}_C(t)$ and graphene:

$$L = r_C(z) - g(z) \qquad \text{(Eq. 4)}$$

where $r_C(z)$ and $g(z)$ means the position of proton and graphyne in z direction.

3. RESULTS AND DISCUSSION

3.1 Graphene with embedded crown ether pores in aqueous environment. The geometry of 18-crown-6 ether pores was taken from previous report[21] and optimized using density functional theory (DFT) calculation. The model systems investigated in this work are based on a 2.4 nm × 2.5 nm graphene sheet containing four 18-crown-6 ether pores, as shown in Figure 1. The sheet was immersed in a periodic aqueous box with initial height of 3.0 nm and water density of 1 g cm^{-3}. Then ReaxFF MD simulation in *NPT* ensemble (P=1 atm, T=300 K) was performed for 2 ns with x and y directions fixed. Afterwards, the system was equilibrated in *NVT* ensemble (T=300 K) for another 2 ns. The detailed system configuration after equilibration can be found in Table S1. Then we analyzed the water/graphene interphase by collecting data from another 1 ns ReaxFF MD simulation in *NVT* ensemble. The water distribution surrounding graphene membrane with embedded crown ether pores is shown in Figure 2a. It can be found that the aqueous phase and graphene membrane are separated by a vacuum zone. In the pore area, the vacuum zone narrowed by still exist. Figure 2b shows the x-z slice of the time-averaged three-dimensional water density at y corresponding to the center of the pore. The height of vacuum zone in graphene area is about 5 Å, and reduces to about 1.5 Å in the pore area. This water distribution is similar with the case of graphyne (n=2) in our previous work[16], in which case protons cannot penetrate the membrane at room temperature for the high energy barrier (16.37 kcal mol^{-1}).

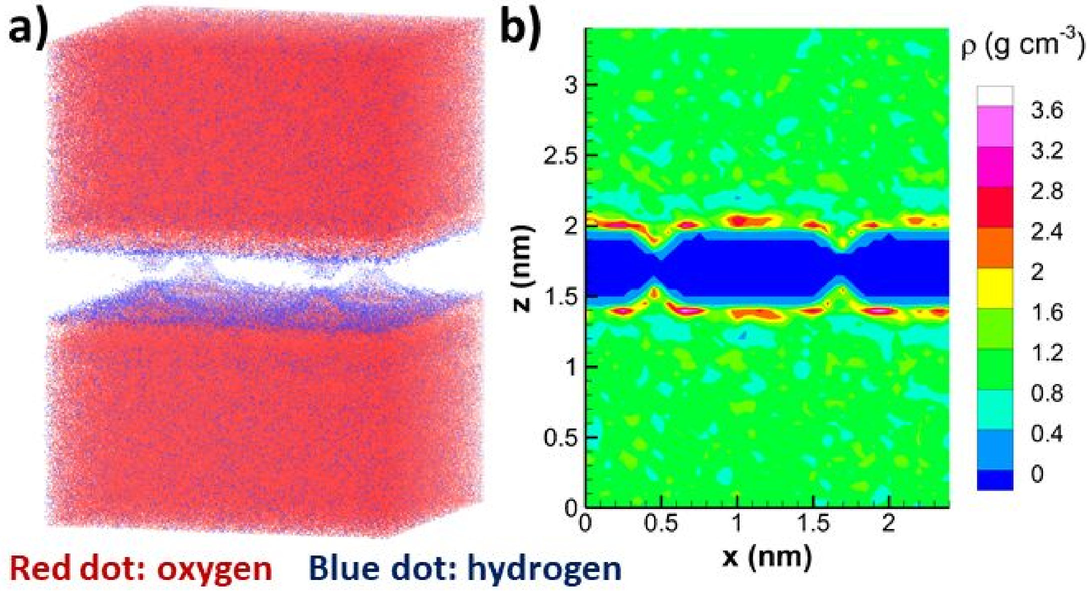

Figure 2. (a) Water distribution surrounding graphene membrane with embedded crown ether pores and (b) *x-z* slice of the time-averaged three-dimensional water density at *y* corresponding to the center of the pore.

3.2 Proton selective conduction behavior. The proton selective conduction behavior across graphene membrane with embedded crown ether pores was studied by ReaxFF MD simulations. As proton-selective conduction is particularly important for DMFC, methanol molecule was chosen to demonstrate the selectivity of graphene-embedded crown ether pores. An extra proton was introduced into the aqueous environment, and 500 ps unbiased ReaxFF MD simulation in *NVT* ensemble was conducted to equilibrate the system. The distance between proton and graphene membrane as a function of time during the equilibration process is shown in Figure S2. It can be found that no proton appeared in the vacuum zone surrounding graphene membrane during the simulation time. Two water molecules in the aqueous system were replaced by a methanol molecule. Then 500 ps unbiased ReaxFF MD simulation in *NVT* ensemble was conducted to equilibrate the system. The distance between the methanol molecule and graphene membrane as a function of time during the equilibration process is shown in Figure S3. Similar with the case of proton, no methanol molecule appeared in the vacuum zone surrounding graphene during the simulation time.

To obtain the proton and methanol penetration energy barriers, we conducted metadynamics simulations. The setup for metadynamics simulations are shown in Figure 3. For proton penetration, as proton mainly exist in the form of hydronium ion (H_3O^+) in aqueous environment, the distance between the oxygen atom in H_3O^+ and graphene membrane was chosen to be the CV. The free energy profile was constructed once all the phase space for the CV have been visited. For methanol penetration, the distance between methanol molecule and graphene membrane was chosen to be the CV. As the mobility of methanol molecule is much lower than proton, taking the same metadynamics setup with proton penetration will result in a large statistical discrepancy. To better evaluate the methanol penetration energy barrier, we took the metadyanmics setup as shown in Figure 3b, where a wall 5 Å away from the top of the simulation box in the *z* direct was added to restrain the methanol molecule movement. The free energy profile was constructed once the methanol molecule penetrates the crown ether pores.

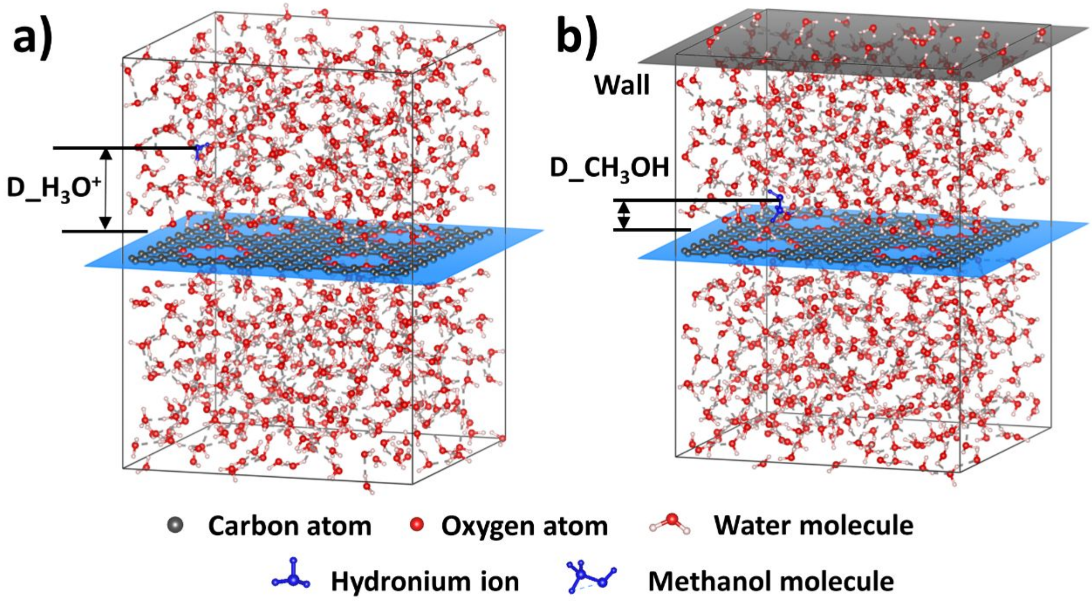

Figure 3. Setup for metadynamics simulations of (a) proton and (b) methanol penetration across the crown ether pores.

For both proton and methanol penetration, we run three metadynamics simulations with different initial geometries. The energy barriers were calculated as the difference between the highest energy value and the lowest energy value. The detailed proton and methanol trajectory and energy profiles for each metadyanmics simulations can be found in Figure S4~S15. The averaged energy barrier for proton conduction across the crown ether pores is 5.53±0.29 kcal mol^{-1} as shown in Figure 4a, which is low enough to occur at room temperature. As the quantum effect of proton is not considered here, the actual proton penetration energy barrier may be even lower[37]. For methanol penetration, the averaged energy barrier was calculated to be 40.94±18.28 kcal mol^{-1}, which is about one order of magnitude higher than the case of proton and hard be overcome at room temperature.

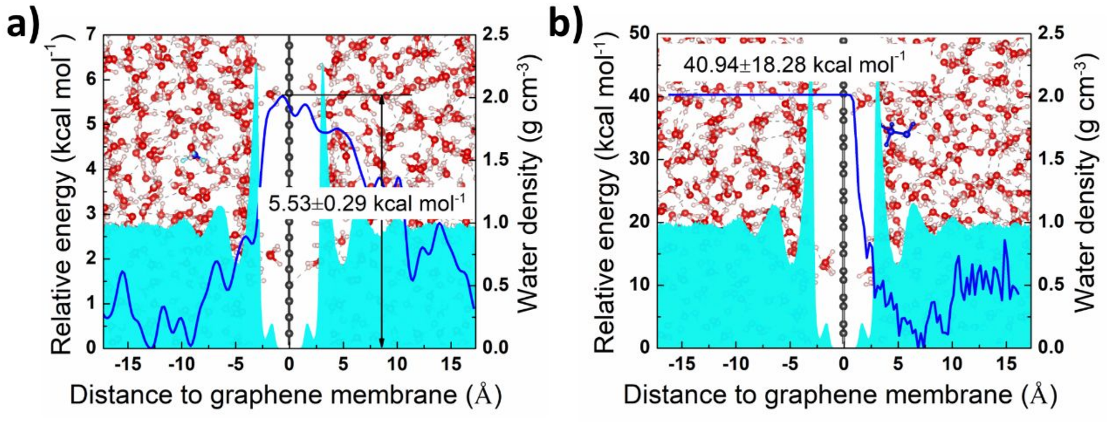

Figure 4. Free energy profiles of (a) proton and (b) methanol as a function of distance to graphene membrane with embedded crown ether pores. The shaded blue area represents water density and the background shows the initial geometries of the simulation system.

Based on the above calculated energy barriers, we can estimate the area-normalized proton conductance across graphene with embedded crown ether pores using the Nernst-Einstein[38-43] relation:

$$\sigma^*_{H^+} = \frac{F^2}{RT} D_{H^+} C_{H^+}/d \quad \text{(Eq. 5)}$$

where F is the Faraday constant, R is the ideal gas constant, T is the temperature, d is the membrane thickness and C_{H^+} is the concentration of proton. D_{H^+} is the diffusion coefficient of proton, which can be estimated using the Einstein-Smoluchowski equation:[40, 42-44]

$$D_{H^+} = \frac{l^2}{\kappa \tau_D} \quad \text{(Eq. 6)}$$

where l is the mean step distance, and κ is a constant depending on the dimensionality of random-walk ($\kappa = 2, 4, \text{or } 6$ for one-, two- and three-dimensional walk). τ_D is the mean time between successive steps, which can be estimated as:[40]

$$\tau_D = {\nu_0}^{-1} \exp\left(\frac{\Delta G}{k_B T}\right) \quad \text{(Eq. 7)}$$

where k_B is the Boltzmann constant, ν_0 is the thermal frequency with $\nu_0 = k_B T/h$, h is the Planck constant, and ΔG is the effective Gibbs free energy of activation for proton diffusion, which we substituted with our calculated energy barriers.

The height of vacuum zone in graphene area is 5.0 Å, which is further used to estimate the membrane thickness and the mean step distance for proton penetration. Here we take $\kappa = 2$ for the penetration process, thus for proton conduction across graphene membrane with embedded crown ether pores at room temperature with proton concentration of 1 M, the estimated area-normalized proton conductance is 3.23×10^5 S cm^{-2}. This conductivity is comparable with our previously predicted graphyne (*n*=3 and *n*=4), and much higher than Nafion[45].

The selectivity of graphene embedded with crown ether pores is estimated using the Arrehnium equation[2, 46] as:

$$S \approx e^{-\frac{\Delta G_{H^+}}{k_B T}} / e^{-\frac{\Delta G_{CH_3OH}}{k_B T}} \quad \text{(Eq. 8)}$$

Substituted with the values obtained from our ReaxFF MD simulations, the selectivity of graphene membrane embedded with crown ether pores is 9.30×10^{25}. This value is high enough to achieve zero-crossover proton exchange membrane for DMFC.

We now discuss the reason for this unexpected high proton conductivity. Figure 5 shows the distance between proton and graphene membrane together with the coordination number between the oxygen atoms in crown ether functional groups and hydrogen element (O_{ether}-H) as a function of metadynamics simulation time. It can be found that every time proton penetrating graphene membrane, the O_{ether}-H coordination number will increase dramatically from 0.1 to a high value between 0.6 and 0.9. This indicate that every time proton penetrating the crown-ether pores, it interacts with the ether functional group, which may help reduce the penetration energy barrier.

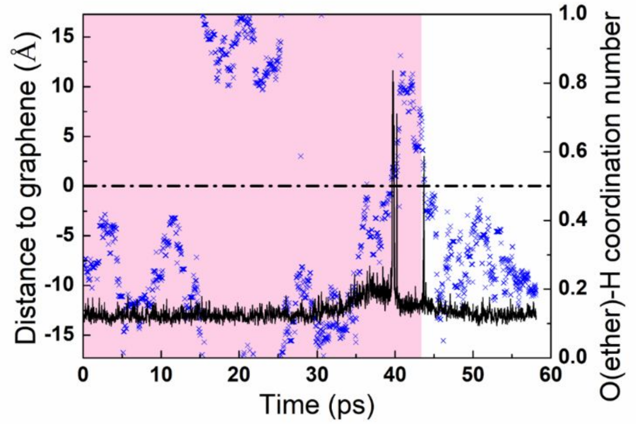

Figure 5. Distance between proton and graphene membrane and coordination number between oxygen atoms in the crown ether functional groups and hydrogen element as a function of simulation time. The pink area represents the data used to construct free energy profile.

We analyzed the proton trajectory for the proton penetration process. It is found that every time proton penetrating crown ether pores, it will approach the oxygen atom in crown ether functional group, as illustrated in Figure 6. The crown ether functional group will serve as a mediator to collect proton from the hydronium ion on one side and pass it to a water molecule on the other side. No direct penetration of hydronium ions has been observed. This behavior significantly lowers the energy barrier for proton penetration across the graphene membrane compared with the cases where proton have to pass through the vacuum zone alone or drag a hydronium ion to the other side.

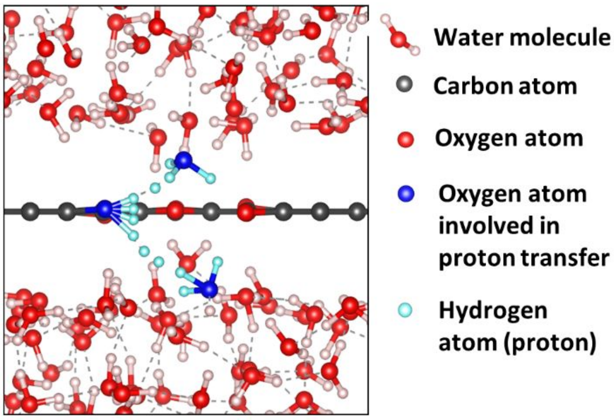

Figure 6. Proposed aqueous proton selective transfer mechanism across crown ether pores.

3.3 Stability of graphene membrane with embedded crown ether pores. In all the above simulations, the position of graphene membrane was fixed for the ease of data analysis. To demonstrate the stability of graphene with embedded crown ether pores in aqueous environment, we performed 1 ns ReaxFF MD simulation in *NVT* ensemble without any restraint. The snapshot after simulation is shown in Figure S16. It can be found that the atomic structure of crown ether pores stays unchanged. Afterwards an extra proton was introduced into the system, and another 1 ns ReaxFF MD simulation without any restraint in *NVT* ensemble was performed. The snapshot after simulation is shown in Figure S17. The appearance of extra proton did not show any influence towards the stability of crown ether pores.

3.4 Graphene pores with other terminations. To further demonstrate the function of crown ether functional group, we investigate the proton transfer process across graphene pores with carbon or hydrogen atom as terminations as shown in Figure 7. For graphene pores terminated with carbon atoms, six carbon atoms were removed from graphene lattice similar with the case of crown ether pores. The detailed geometry was taken from the experimentally observed stable configuration[47] and optimized using DFT calculations. When putting it into the aqueous environment, water molecules around the pores will dissociate into hydroxyl groups and hydrogen atoms bonded with the carbon atoms in a short time within 5 ps as shown in Figure S18, indicating that graphene pores terminated with carbon atoms are not stable in aqueous environment.

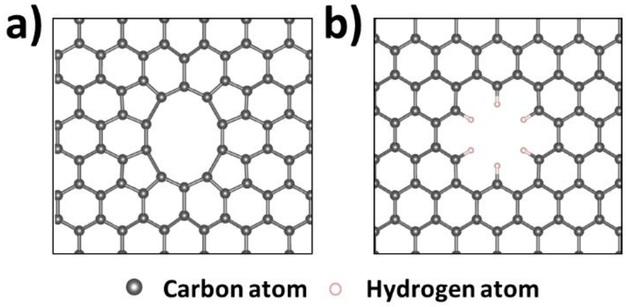

Figure 7. Geometries of graphene pores terminated with (a) carbon and (b) hydrogen atoms.

To construct graphene pores terminated with hydrogen atoms, the oxygen atoms in crown ether pores were replaced with carbon atoms, and each carbon atom was bonded with a hydrogen atom. Then we studied the proton penetration behavior across the graphene pores using metadyanmics simulations. As the proton penetration energy barrier across the graphene pores terminated with hydrogen atoms are very high, when using the same metadyanmics simulation setup as the crown-ether pores, no proton penetration behavior can be captured when the deposited bias potential reaches as high as 25 kcal mol^{-1}. Due to the complexity of the CV used, further deposition of bias potential will result in the self-dissociation of water molecules and no meaningful results can be obtained. To better evaluate the penetration energy barrier, we took the metadynamics simulation setup similar with our previous work when dealing with graphyne (n=1) as shown in Figure 8a.[16] All the O-H bonds in water molecules were constrained when the bond lengths exceed 1.4 Å and a pair of walls were put 5 Å away from the graphene membrane to confine the proton movement. The distance between the extra proton and graphene was used as CV. The energy profiles were constructed once the proton penetrate the graphene pores from one to the other side. The detailed proton trajectory and energy profiles for each metadyanmics simulation can be found in Figure S19-S24. The averaged energy barrier for proton conduction across the graphene pores terminated with hydrogen atoms is 158.52±58.92 kcal mol^{-1} as shown in Figure 8b, which is about thirty times of that for proton penetration across crown ether pores.

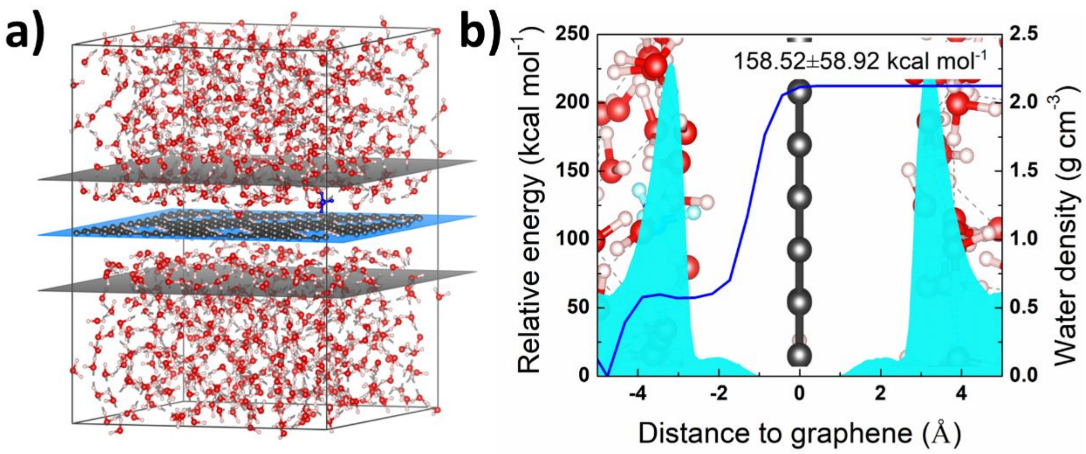

Figure 8. (a) Setup for metadynamics simulations of proton penetration across hydrogen terminated pores and (b) free energy profiles of proton as a function of distance to graphene membrane. The shaded blue area represents water density and the background shows the initial geometries of the simulation system.

4. CONCLUSIONS

In this work we investigated the proton selective conduction behavior across graphene-embedded 18-crown-6 ether pores using extensive ReaxFF MD simulations. It is found that though there exist a vacuum gap between the aqueous phase and graphene, the proton conduction behavior can be mediated by the crown ether functional groups, leading to a low proton penetration energy barrier of 5.53±0.29 kcal mol^{-1}. In the meantime, the vacuum gap as well as the small pore size can effectively block the penetration of other molecules such as methanol. The proton conductivity for graphene with embedded crown ether pores is estimated to be 3.23×10^{5} S cm^{-2}, and its selectivity towards methanol is estimated to be 9.30×10^{25}. Our work demonstrated the significant influence of pore edge functional groups on the proton-selective conduction behavior, and proposed that graphene with embedded 18-crown-6 pores can provide a high proton conductivity and an ultrahigh selectivity simultaneously, which shed light on the future design of zero-crossover proton exchange membrane.

ASSOCIATED CONTEST

Supporting Information

Supplementary details of the simulated systems, methods and additional results and discussion. (PDF)

AUTHOR INFORMATION

Corresponding Author

*E-mail: le.shi@mail.xjtu.edu.cn

ORCID

Le Shi: 0000-0003-1468-4549

Ao Xu: 0000-0003-0648-2701

Notes

The authors declare no competing financial interest.

ACKNOWLEDGMENTS

The work described in this paper was supported by National Natural Science Foundation of China (51907159) and Young Talent Recruiting Plans of Xi'an Jiaotong University (DQ6J002). The simulations were carried out at LvLiang Cloud Computing Center of China, and were performed on TianHe-2.

Notes

The authors declare no competing financial interest

REFERENCES

[1] Novoselov, K. S.; Geim, A. K.; Morozov, S. V.; Jiang, D.; Zhang, Y.; Dubonos, S. V.; Grigorieva, I. V.; Firsov, A. A. Electric Field Effect in Atomically Thin Carbon Films. *Science* **2004**, *306*, 666-669.

[2] Wang, L.; Boutilier, M. S.; Kidambi, P. R.; Jang, D.; Hadjiconstantinou, N. G.; Karnik, R. Fundamental Transport Mechanisms, Fabrication and Potential Applications of Nanoporous Atomically Thin Membranes. *Nat. Nanotech*. **2017**,*12*, 509.

[3] Mi, B. Scaling Up Nanoporous Graphene Membranes. Science, 364, 1033-1034.

[4] Prozorovska, L.; Kidambi, P. R. State-of-the-Art and Future Prospects for Atomically Thin Membranes from 2D Materials. *Adv. Mater*. **2018**, *30*, 1801179.

[5] Li, H.; Song, Z.; Zhang, X.; Huang, Y.; Li, S.; Mao, Y.; Ploehn, H. J.; Bao, Y.; Yu, M. Ultrathin, Molecular-Sieving Graphene Oxide Membranes for Selective Hydrogen Separation. *Science* **2013**, *342*, 95-98.

[6] Surwade, S. P.; Smirnov, S. N.; Vlassiouk, I. V.; Unocic, R. R.; Veith, G. M.; Dai, S.; Mahurin, S. M. Water Desalination Using Nanoporous Single-Layer Graphene. *Nat. Nanotech*. **2015**, *10*, 459.

[7] Fang, A.; Kroenlein, K.; Riccardi, D.; Smolyanitsky, A. Highly Mechanosensitive Ion Channels from Graphene-Embedded Crown Ethers. *Nat. Mater*. **2019**, *18*, 76.

[8] Hu, S.; Lozada-Hidalgo, M.; Wang, F. C.; Mishchenko, A.; Schedin, F.; Nair, R. R.; Hill, E. W.; Boukhvalov, D. W.; Katsnelson, M. I.; Dryfe, R. A.; *et al*. Proton Transport Through One-Atom-Thick Crystals. *Nature*. **2014**, *516*, 227.

[9] Neburchilov, V.; Martin, J.; Wang, H.; Zhang, J. A Review of Polymer Electrolyte Membranes for Direct Methanol Fuel Cells. *J. Power Sources* **2007**, *169*, 221-238.

[10] Yan, X. H.; Wu, R.; Xu, J. B.; Luo, Z.; Zhao, T. S. A Monolayer Graphene–Nafion Sandwich Membrane for Direct Methanol Fuel Cells. *J. Power Sources* **2016**, *311*, 188-194.

[11] Holmes, S. M.; Balakrishnan, P.; Kalangi, V. S.; Zhang, X.; Lozada-Hidalgo, M.; Ajayan, P. M.; Nair, R. R. 2D Crystals Significantly Enhance the Performance of a Working Fuel Cell. *Adv. Energy Mater*. **2017**, *7*, 1601216.

[12] Yoon, S. I.; Seo, D. J.; Kim, G.; Kim, M.; Jung, C. Y.; Yoon, Y. G.; Joo, S. H.; Kim, T. Y.; Shin, H. S. AA′-Stacked Trilayer Hexagonal Boron Nitride Membrane for Proton Exchange Membrane Fuel Cells. *ACS Nano* **2018**, *12*, 10764-10771.

[13] Shi, L.; Xu, A.; Chen, G.; Zhao, T. S. Theoretical Understanding of Mechanisms of Proton Exchange Membranes Made of 2D Crystals with Ultrahigh Selectivity. *J. Phys. Chem. Lett*. **2017**, *8*, 4354-4361.

[14] Feng, Y.; Chen, J.; Fang, W.; Wang, E. G.; Michaelides, A.; Li, X. Z. Hydrogenation Facilitates Proton Transfer through Two-Dimensional Honeycomb Crystals. *J. Phys. Chem. Lett*. **2017**, *8*, 6009-6014.

[15] Achtyl, J. L.; Unocic, R. R.; Xu, L.; Cai, Y.; Raju, M.; Zhang, W.; Sacci, R. L.; Vlassiouk, I. V.; Fulvio, P. F.; Ganesh, P.; *et al*. Aqueous Proton Transfer across Single-Layer Graphene. *Nat. Commun*. **2015**, *6*, 6539.

[16] Shi, L.; Xu, A.; Pan, D.; Zhao, T. S. Aqueous Proton-Selective Conduction across Two-Dimensional Graphyne. *Nat. Commun*. **2019**, *10*, 1165.

[17] Moreno, C.; Vilas-Varela, M.; Kretz, B.; Garcia-Lekue, A.; Costache, M. V.; Paradinas, M.; Panighel, M.; Ceballos, G.; Valenzuela, S. O.; Peña, D.; *et al*. Bottom-Up Synthesis of Multifunctional Nanoporous Graphene. *Science* **2018**, *360*, 199-203.

[18] Liu, W.; Luo, X.; Bao, Y.; Liu, Y. P.; Ning, G. H.; Abdelwahab, I.; Li, L.; Nai, C. T.; Hu, Z. G.; Zhao, D.; *et al*. A Two-Dimensional Conjugated Aromatic Polymer via C–C Coupling Reaction. *Nat. Chem.* **2017**, *9*, 563.

[19] He, Z.; Zhou, J.; Lu, X.; Corry, B. Bioinspired Graphene Nanopores with Voltage-Tunable Ion Selectivity for Na^+ and K^+. *ACS Nano* **2013**, *7*, 10148-10157.

[20] Guo, J.; Lee, J.; Contescu, C. I.; Gallego, N. C.; Pantelides, S. T.; Pennycook, S. J.; Moyer, B. A.; Chisholm, M. F. Crown Ethers in Graphene. *Nat. Commun*. **2014**, *5*, 5389.

[21] Smolyanitsky, A.; Paulechka, E.; Kroenlein, K. Aqueous Ion Trapping and Transport in Graphene-Embedded 18-Crown-6 Ether Pores. *ACS Nano* **2018**, *12*, 6677-6684.

[22] Sahu, S.; Elenewski, J.; Rohmann, C.; Zwolak, M. Optimal Transport and Colossal Ionic Mechano-Conductance in Graphene Crown Ethers. *Sci. Adv*. **2019**, *5*, eaaw5478.

[23] Zhang, W.; Van Duin, A. C. Improvement of the ReaxFF Description for Functionalized Hydrocarbon/Water Weak Interactions in the Condensed Phase. *J. Phys. Chem. B* **2018**, *122*, 4083-4092.

[24] Zhang, W.; Chen, X.; Van Duin, A. C. Isotope Effects in Water: Differences of Structure, Dynamics, Spectrum, and Proton Transport Between Heavy and Light Water from ReaxFF Reactive Force Field Simulations. *J. Phys. Chem. Lett*. **2018**, *9*, 5445-5452.

[25] Hassanali, A.; Giberti, F.; Cuny, J.; Kühne, T. D.; Parrinello, M. Proton Transfer through the Water Gossamer. *Proc. Natl. Acad. Sci*. **2013**, *110*, 13723-13728.

[26] Gonze, X.; Beuken, J. M.; Caracas, R.; Detraux, F.; Fuchs, M.; Rignanese, G. M.; Sindic, L.; Verstraete, M.; Zerah, G.; Jollet, F.; *et al*. First-Principles Computation of Material Properties: the ABINIT Software Project. *Comput. Mater. Sci.* **2002**, *25*, 478-492.

[27] Gonze, X.; Amadon, B.; Anglade, P. M.; Beuken, J. M.; Bottin, F.; Boulanger, P.; Bruneval, F.; Caliste, D.; Caracas, R.; Côté, M.; *et al*. ABINIT: First-Principles Approach to Material and Nanosystem Properties. *Comput. Phys. Commun*. **2009**, *180*, 2582-2615.

[28] Gonze, X. A Brief Introduction to the ABINIT Software Package. *Z. Kristallogr*. **2005**, *220*, 558-562.

[29] Perdew, J. P.; Ernzerhof, M.; Burke, K. Rationale for Mixing Exact Exchange with Density Functional Approximations. *J. Chem. Phys.* **1996**, *105*, 9982-9985.

[30] Blöchl, P. E. Projector Augmented-Wave Method. Phys. Rev. B 1994, 50, 17953.

[31] Plimpton, S. Fast Parallel Algorithms for Short-Range Molecular Dynamics. *J. Comput. Phys.* **1995**, *117*, 1-9.

[32] Aktulga, H. M.; Fogarty, J. C.; Pandit, S. A.; Grama, A. Y. Parallel Reactive Molecular Dynamics: Numerical Methods and Algorithmic Techniques. *Parallel Comput.* **2012**, *38*, 245-259.

[33] Laio, A.; Parrinello, M. Escaping Free-Energy Minima. *Proc. Natl. Acad. Sci*. **2002**, *99*, 12562-12566.

[34] Bonomi, M.; Branduardi, D.; Bussi G.; Camilloni C.; Provasi, D.; Raiteri, P.; Donadio, D.; Marinelli, F.; Pietrucci, F.; Broglia, R. A. et al. PLUMED: A Portable Plugin for Free-Energy Calculations with Molecular Dynamics. *Comput. Phys. Commun.* **2009**, *180*, 1961–1972.

[35] Park, J. M.; Laio, A.; Iannuzzi, M.; Parrinello, M. Dissociation Mechanism of Acetic Acid in Water. *J. Am. Chem. Soc*. **2006,** *128*, 11318-11319.

[36] Zhang, C.; Knyazev, D. G.; Vereshaga, Y. A.; Ippoliti, E.; Nguyen, T. H.; Carloni, P.; Pohl, P. Water at Hydrophobic Interfaces Delays Proton Surface-to-Bulk Transfer and Provides a Pathway for Lateral Proton Diffusion. *Proc. Natl. Acad. Sci*. **2012**, *109*, 9744-9749.

[37] Ekanayake, N. T.; Huang, J.; Jakowski, J.; Sumpter, B. G.; Garashchuk, S. Relevance of the Nuclear Quantum Effects on the Proton/Deuteron Transmission through Hexagonal Boron Nitride and Graphene Monolayers. *J. Phys. Chem. C*. **2017**, *121*, 24335-22344.

[38] Prentice, G. Electrochemical Engineering Principles. Prentice-Hall, Inc.: Englewood Cliffs, NJ, **1991**

[39] Bockris, J.O'. M.; Reddy, A.K.N. Modern Eletrochemistry, 1 Ionics. Plenum Press: New York, **1998**

[40] Choi, P.; Jalani, N. H.; Datta, R. Thermodynamics and Proton Transport in Nafion II. Proton Diffusion Mechanisms and Conductivity. *J. Electrochem. Soc*. **2005**, *152*, E123-E130.

[41] Videa, M.; Xu, W.; Geil, B.; Marzke, R.; Angell, C. A. High Li^+ Self-Diffusivity and Transport Number in Novel Electrolyte Solutions. *J. Electrochem. Soc*. **2001**, *148*, A1352-A1356.

[42] MacFarlane, D. R.; Forsyth, M.; Izgorodina, E. I.; Abbott, A. P.; Annat, G.; Fraser, K. On the Concept of Ionicity in Ionic Liquids. *Phys. Chem. Chem. Phys*. **2009**, *11*, 4962-4967.

[43] Sangoro, J. R.; Serghei, A.; Naumov, S.; Galvosas, P.; Kärger, J.; Wespe, C.; Bordusa, F.; Kremer, F. Charge Transport and Mass Transport in Imidazolium-Based Ionic Liquids. *Phys. Rev. E* **2008**, *77*, 051202.

[44] Philibert, J. Atom Movements: Diffusion and Mass Transport in Solids, Les Éditions de Physique: Les Ulis, **1991**

[45] Mauritz, K. A.; Moore, R. B. State of Understanding of Nafion. *Chem. Rev*. **2010**, *104*, 4535–4586.

[46] Blankenburg, S.; Baieri, M.; Fasel, R.; Müllen, K.; Pignedoli, C. A.; Passerone, D. Porous Graphene as an Atmospheric Nanofilter. *Small* **2010**, *6*, 2266-2271.

[47] Robertson, A. W.; Lee, G. D.; He, K.; Gong, C.; Chen, Q.; Yoon, E.; Kirkland, A. I.; Warner, J. H. Atomic Structure of Graphene Subnanometer Pores. *ACS Nano* **2015**, *9*, 11599-11607.

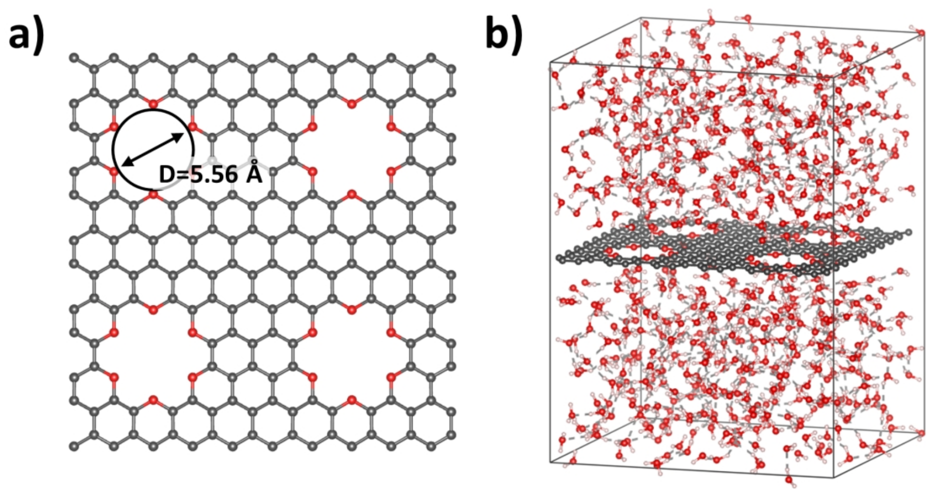

Geometry of graphene embedded 18-crown-6 ether pores in (a) vacuum and (b) aqueous environment.

177x99mm (300 x 300 DPI)

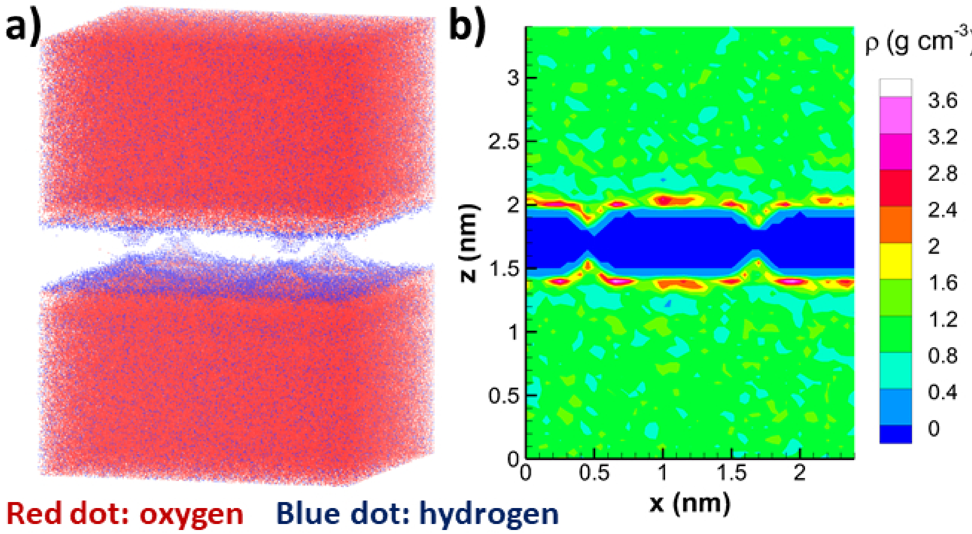

(a) Water distribution surrounding graphene membrane with embedded crown ether pores and (b) x-z slice of the time-averaged three-dimensional water density at y corresponding to the center of the pore.

177x100mm (96 x 96 DPI)

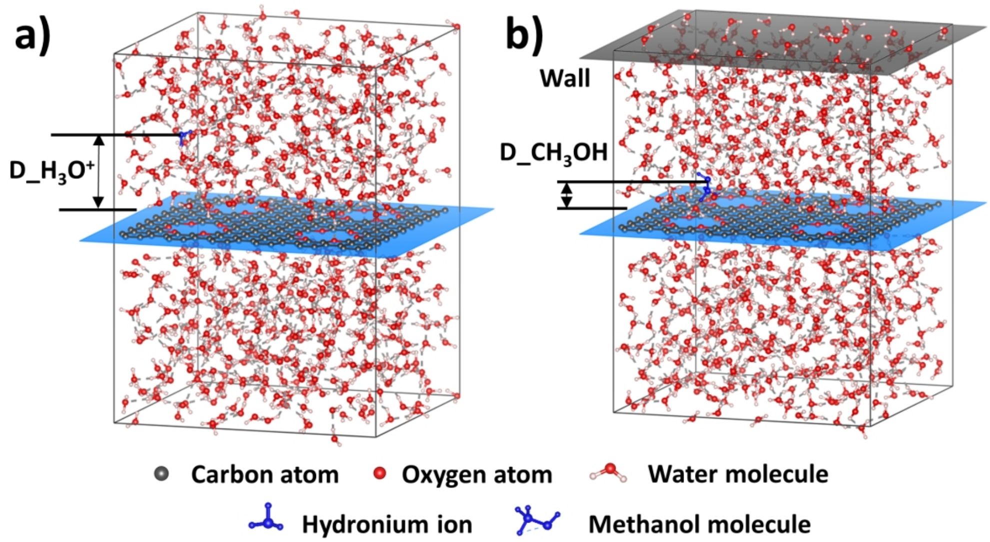

Setup for metadynamics simulations of (a) proton and (b) methanol penetration across the crown ether pores.

177x99mm (300 x 300 DPI)

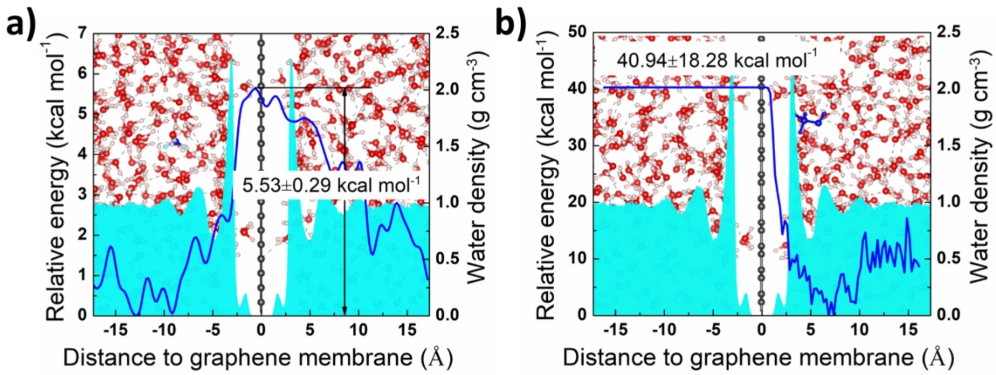

Free energy profiles of (a) proton and (b) methanol as a function of distance to graphene membrane with embedded crown ether pores. The shaded blue area represents water density and the background shows the initial geometries of the simulation system.

177x70mm (300 x 300 DPI)

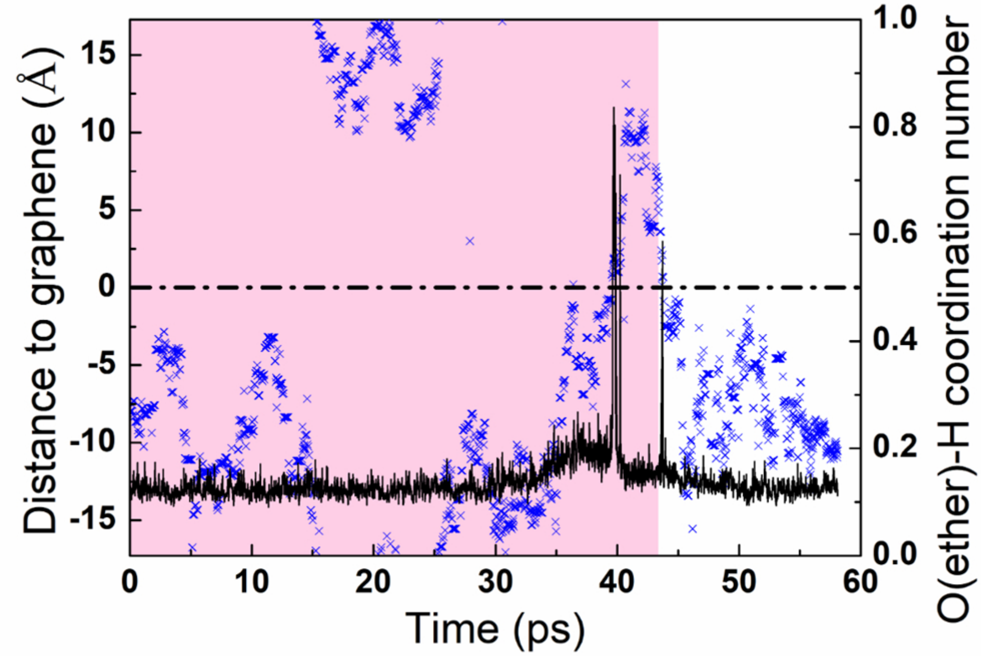

Distance between proton and graphene membrane and coordination number between oxygen atoms in the crown ether functional groups and hydrogen element as a function of simulation time. The pink area represents the data used to construct free energy profile.

84x60mm (300 x 300 DPI)

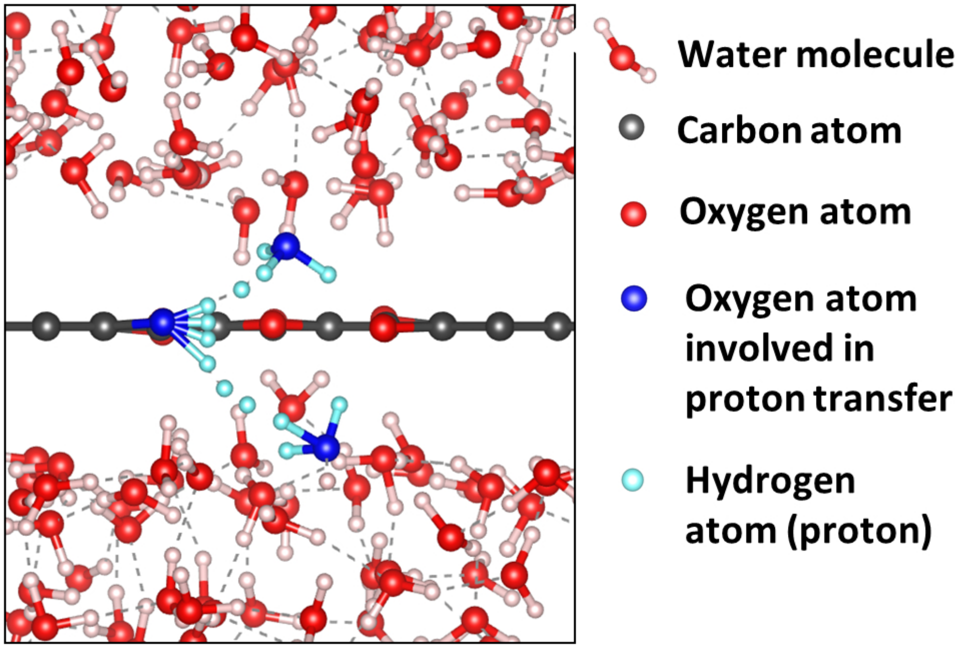

Proposed aqueous proton selective transfer mechanism across crown ether pores.

84x60mm (300 x 300 DPI)

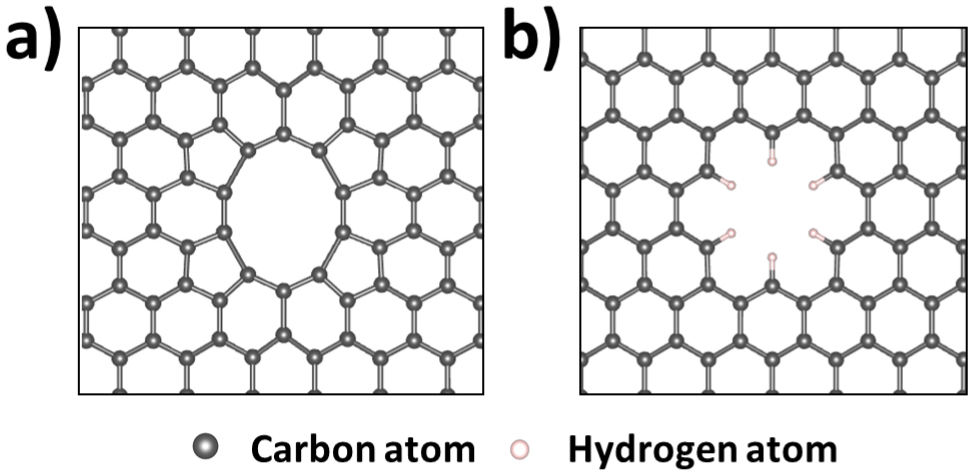

Geometries of graphene pores terminated with (a) carbon and (b) hydrogen atoms.

84x44mm (300 x 300 DPI)

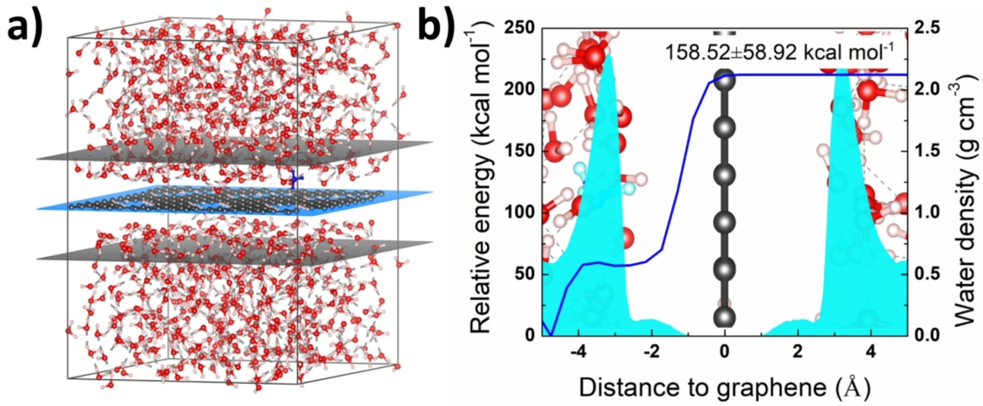

(a) Setup for metadynamics simulations of proton penetration across hydrogen terminated pores and (b) free energy profiles of proton as a function of distance to graphene membrane. The shaded blue area represents water density and the background shows the initial geometries of the simulation system.

177x80mm (300 x 300 DPI)